Physiological Measurement

Detection of brain oedema using magnetic induction tomography: a feasibility study of the likely sensitivity and detectability

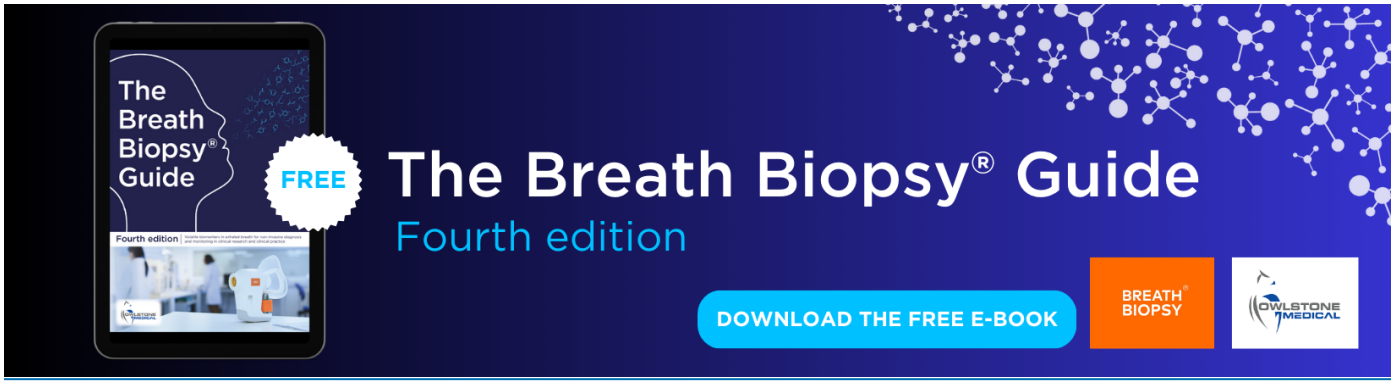

INSTITUTE OF PHYSICS PUBLISHING PHYSIOLOGICAL MEASUREMENT

Physiol. Meas. **25** (2004) 347–354 PII: S0967-3334(04)66894-8

Detection of brain oedema using magnetic induction tomography: a feasibility study of the likely sensitivity and detectability

Robert Merwa[1], Karl Hollaus[2], Oszkar Biró[2] and Hermann Scharfetter [1]

[1] Institute for Biomedical Engineering, Graz University of Technology, Inffeldgasse 18, A-8010 Graz, Austria
[2] Institute for Fundamentals and Theory in Electrical Engineering, Graz University of Technology, Kopernikusgasse 24, A-8010 Graz, Austria

E-mail: merwa@bmt.tu-graz.ac.at

Received 31 July 2003, accepted for publication 12 November 2003
Published 3 February 2004
Online at stacks.iop.org/PM/25/347 (DOI: 10.1088/0967-3334/25/1/038)

Abstract

The detection and continuous monitoring of brain oedema is of particular interest in clinical applications because existing methods (invasive measurement of the intracranial pressure) may cause considerable distress for the patients. A new non-invasive method for continuous monitoring of an oedema promises the use of multi-frequency magnetic induction tomography (MIT). MIT is an imaging method for reconstructing the changes of the conductivity $\Delta\kappa$ in a target object. The sensitivity of a single MIT-channel to a spherical oedematous region was analysed with a realistic model of the human brain. The model considers the cerebrospinal fluid around the brain, the grey matter, the white matter, the ventricle system and an oedema (spherical perturbation). Sensitivity maps were generated for different sizes and positions of the oedema when using a coaxial coil system. The maps show minimum sensitivity along the coil axis, and increasing values when moving the perturbation towards the brain surface. Parallel to the coil axis, however, the sensitivity does not vary significantly. When assuming a standard deviation of 10^{-7} for the relative voltage change due to the system's noise, a centrally placed oedema with a conductivity contrast of 2 with respect to the background and a radius of 20 mm can be detected at 100 kHz. At higher frequencies the sensitivity increases considerably, thus suggesting the capability of multi-frequency MIT to detect cerebral oedema.

Keywords: magnetic induction tomography, eddy currents, finite elements, sensitivity distribution, human brain, oedema

1. Introduction

Neurological aggravations of patients with an acute cerebral circulation impairment (craniocerebral injury) can trace back to a swelling of the brain. The survey of such patients is carried out with pressure sensors directly in the brain in combination with imaging techniques such as CT or MR. These methods can cause considerable distress; thus new continuous methods are required. In this context magnetic induction tomography (MIT) appears attractive. MIT is a non-invasive and contactless imaging method for reconstructing the changes $\Delta\kappa$ of the complex conductivity distribution $\kappa = \sigma + j\omega\epsilon$ in a target object (Griffiths 2001, Griffiths *et al* 1999, Korjenevsky and Cherepenin 1999, Korjenevsky *et al* 2000, Peyton *et al* 1995). Magnetically coupled conductivity sensors (Netz *et al* 1993), specifically when applied at multiple frequencies (Scharfetter *et al* 2003), appear especially attractive for the monitoring of pathologies in the brain, which are correlated with local fluid shifts, e.g., oedema (Kao *et al* 1991), haemorrhages or epileptic events. To this end, a sinusoidal time varying magnetic field B_0 generated by an excitation coil penetrates the object under investigation. Eddy currents are induced, perturbing the primary field B_0. A change $\Delta\kappa$ of the conductivity results in an additional perturbation ΔB of B_0. The corresponding voltages ΔV and V_0 induced in a receiver coil carry information about the conductivity distribution, which is essential for the solution of the inverse problem. This paper is dedicated to analysing the sensitivity of the method with a realistic electromagnetic model of the human brain. Questions of particular interest are: (a) what is the detectible size of an oedema when assuming a certain conductivity change? (b) How does the sensitivity of a coaxial measurement channel vary with the position of the oedema?

2. Methods

2.1. Modelling environment

The boundary value problem to be solved is a time harmonic eddy current problem in the steady state excited by coils described by Maxwell's equations and the associated constitutive laws. This problem is solved with the finite element (FE) method. The complex A_r, $V - A_r$ formulation (Biro 1999) was employed, A_r denoting a reduced magnetic vector potential valid in the entire problem region and V being the modified electric scalar potential applied in the conducting region only. A_r is approximated by edge basis functions and the modified electric scalar potential V is represented by nodal basis functions.

The solver was first checked with typical benchmark problems, comparing the performance with that of the previously developed and exhaustively tested software package 'EleFAnT3D' (developed at the Institute for Fundamentals and Theory in Electrical Engineering, Graz University of Technology). The deviation of the magnetic flux density and the eddy currents on several models (e.g., conducting cube within a cylindrical coil and Nakata plate) were in the range of 2%. The implementation of this FE-solver has been described in detail in Hollaus *et al* (2002) and for the experimental validation simulated and measured data of a tank phantom with two compartments were compared (Merwa *et al* 2003).

The segmentation was performed manually with custom-made software written in Matlab (The MathWorks Inc.) by picking base points for each boundary in each picture. Parametric natural cubic splines are used to interpolate the anatomical boundaries with a low number of base points. The result is a set of points, which describe the geometry in 3D, as shown in figure 1.

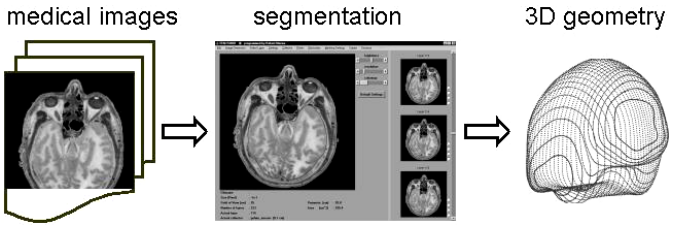

Figure 1. Flow diagram of the segmentation process.

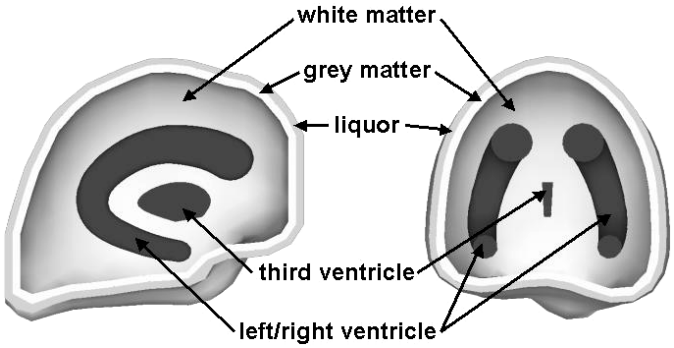

Figure 2. Sagittal and coronal sectional view of the brain model.

Figure 2 shows a sagittal and coronal sectional view of the complete brain model. The outer boundary of the grey matter was extracted from about 150 images of the human head from the Visible Man Human Project database (NPAC/OLDA Visible Human Viewer). The border of the white matter and the cerebrospinal fluid around the brain were not segmented but calculated by assuming a constant thickness of the cerebrospinal fluid and the grey matter. This approximation is acceptable because these structures are very thin in comparison with the white matter and small inaccuracies in their geometry will not affect the basic sensitivity analysis significantly. Furthermore the sulci of the human cortex were disregarded, because they are filled with cerebrospinal fluid, which represents a conducting bridge for the eddy currents that flow approximately parallel to the brain surface. The surface of the ventricle system (left, right and third ventricle) was generated artificially in order to manipulate their size and orientation in an easy way.

The central user interface of our software allows for manipulating interactively the whole brain geometry, e.g., the thickness of the cerebrospinal fluid around the brain and/or the grey matter and the morphology of the ventricle system. A defined spherical perturbation can be set interactively simulating an oedema in the brain. The software includes a bidirectional interface to the mesh generator HyperMesh (Altair Inc.) and to the eddy current solver. Sensitivity analysis is then carried out by automatic displacement and changes of the size of the perturbation.

2.2. Analysis of sensitivity and detectability

For a first analysis the ventricle system was omitted. The simulation arrangement is depicted in figure 3. A cylindrical excitation coil with an outer diameter $d_a = 95$ mm, a height $h = 18$ mm and $n = 45$ turns was modelled. The excitation current was set to 1 A and the excitation

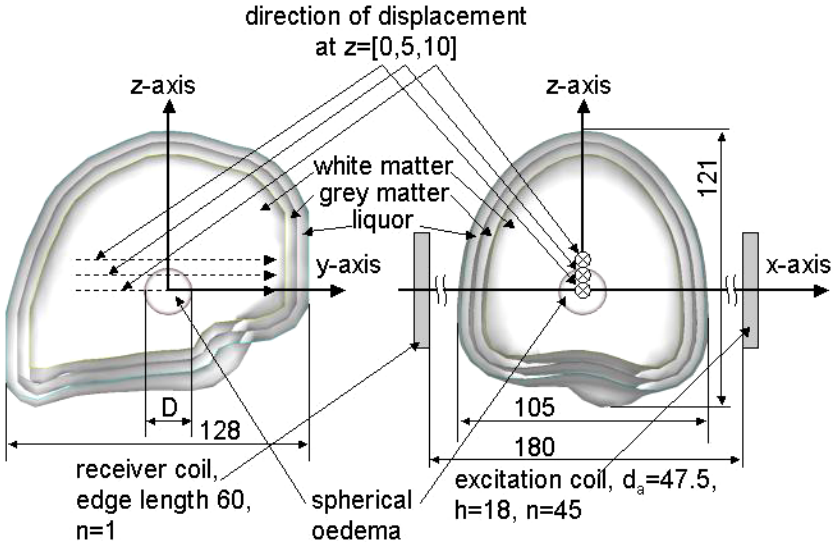

Figure 3. Simulation arrangement, all measurements in mm.

Table 1. Number of FEs of the used brain structures.

Structure	Number of FEs
Cerebrospinal fluid	∼4000
Grey matter	∼3500
White matter	∼7000
Perturbation	∼600

frequency was set to 100 kHz. The receiver consists of a quadratic coil with 1 turn and an edge length of 60 mm. The coils were positioned about 40 mm left and right of the surface of the cerebrospinal fluid. The thickness of the cerebrospinal fluid and the grey matter was set to 5 mm, and the spherical perturbation was placed inside the white matter. In table 1 the numbers of finite elements of the used structures are listed. The magnetic flux density of the excitation coil was calculated with Biot–Savart's law in the 'infinite space', however, without considering propagation delays. The normal component of the B field was assumed to vanish on the far boundary which was approximated surrounding the brain with a sphere consisting of about 33 000 FEs.

The change of the received voltage was simulated while:

(a) performing a 2D-sweep, thus generating a sensitivity map at a height of $z = 10$ mm. Δx and Δy were selected with 5 mm and the diameter of the perturbation was set to 30 mm;
(b) displacing the spherical perturbation with a diameter of 20 along the y-axis at $x = 0$ and $z = 0$, 5 and 10 mm;
(c) changing the diameter D of the perturbation from 20 up to 50 mm in steps of 2 mm at the central position $x = 0$, $y = 0$ and $z = 10$. This central position was chosen, because here the sensitivity has a minimum value and represents the worst case.

For all simulations, the excitation coil and the receiver coil were kept coaxial with the spherical perturbation. In table 2 the tissue parameters (conductivity σ, relative permittivity ε_r) of the used structures are listed. To obtain the conductivity and the relative permittivity of different tissue types at defined frequencies, the parametric model described in Gabriel *et al* (1996)

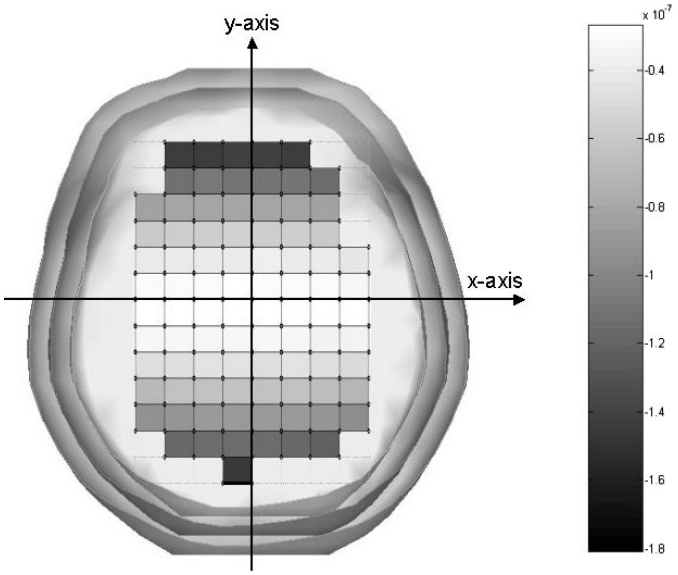

Figure 4. Im(SCR) mapping ($\Delta x = \Delta y = 5$ mm) with a perturbation diameter of 30 mm.

Table 2. Tissue parameters of the used brain structures.

Structure	σ (S m^{-1})	ε_r
Cerebrospinal fluid	1.6	200
Grey matter	0.134	3222
White matter	0.082	2107
Perturbation	0.164	1000

was used. The oedema was assumed to be extracellular, hence increasing the conductivity at low frequencies. Exact tissue parameters of an extracellular oedema are not well established in the literature, hence they were assumed with the help of the measurement results for an intracellular oedema published in Lingwood *et al* (2002). The central hypothesis is that the β-dispersion changes in a characteristic way during a change of the tissue hydration. Accordingly the conductivity of the oedema was assumed as twice the conductivity of the white matter and the relative permittivity was set to about half the value of the white matter.

According to previous publications (Scharfetter *et al* 2002), the perturbation of the received voltage was quantified in terms of SCR $= \Delta V / V_0$ (signal/carrier ratio). ΔV was defined as the difference between the induced voltages in the perturbed and unperturbed cases. In order to avoid discretization errors the same mesh was used for the perturbed and unperturbed models.

3. Results

(a) Figure 4 shows the sensitivity map with $\Delta x = \Delta y = 5$ mm at $z = 10$ mm. The diameter of the spherical perturbation was set to 30 mm. Figures 5 and 6 depict several profiles of this map along the y-axis and the x-axis, respectively.

The variation of the Im(SCR), when displacing the sphere parallel to the y-axis (figure 5), was 10 times higher than during a movement in the direction of the coil axis

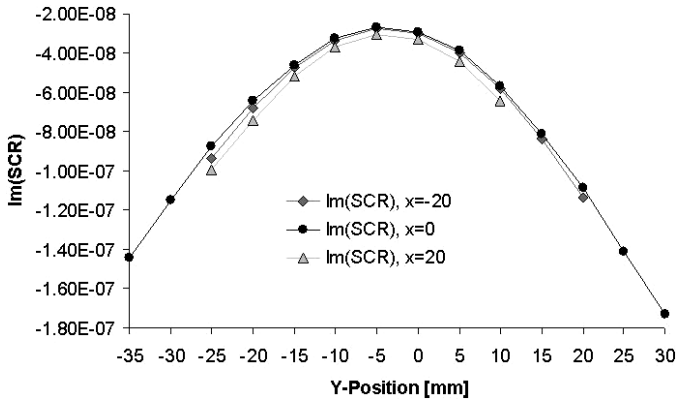

Figure 5. Particular profiles along the *y*-axis.

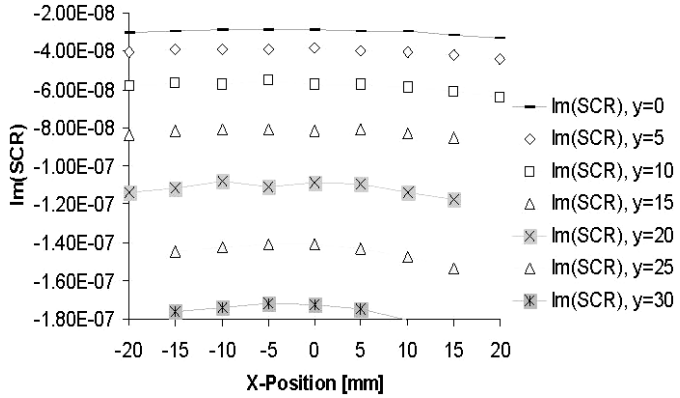

Figure 6. Particular profiles along the *x*-axis.

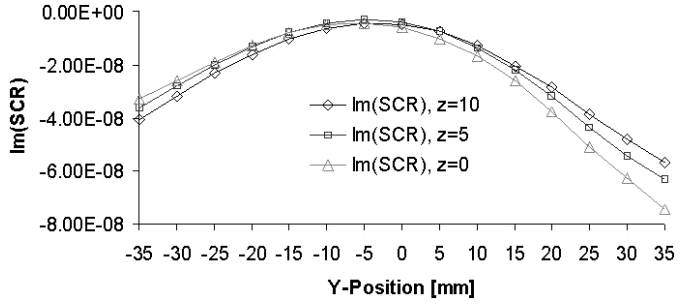

Figure 7. Im(SCR) along the *y*-axis with a perturbation diameter of 20 mm at different *z*-levels.

(figure 6). This effect depends on the size of the receiver coils and will be investigated in detail by means of future simulations.

(b) Figure 7 depicts the simulated Im(SCR) at different *z*-levels when displacing the spherical perturbation with a diameter of 20 mm along the *y*-axis.

The simulation results show very good qualitative agreement with the experimental and simulated results for a cylindrical model (Merwa *et al* 2003, Scharfetter *et al* 2002).

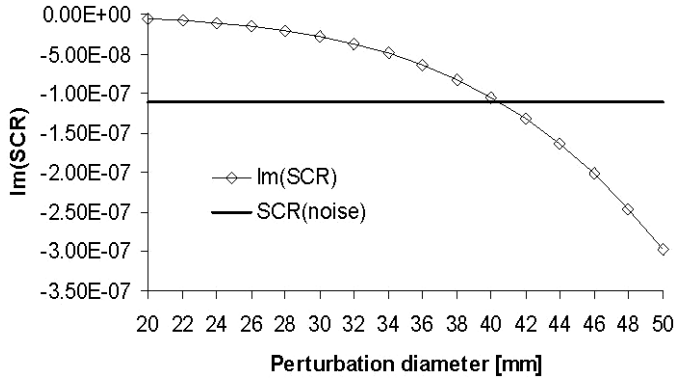

Figure 8. Im(SCR) versus perturbation diameter.

A clear minimum of the absolute value of the Im(SCR) can be seen near the centre. The asymmetry subject to the position $y = 0$ is caused by slightly asymmetric boundaries of the brain. If the perturbation comes closer to the bounding surface, the absolute value of Im(SCR) increases due to larger eddy current densities in these regions. This is clearly visible in figure 7. At $y = 35$ mm the sphere approaches the border (see figure 3) at the bottom of the brain while moving from $z = 10$ towards $z = 0$, hence increasing the absolute value of Im(SCR). At $y = -35$, in contrast, the sphere moves away from the border, thus producing the opposite effect.

(c) Figure 8 shows the simulated Im(SCR) depending on a change of the diameter of the perturbed sphere.

The increase of the absolute value of the Im(SCR) with the diameter of the perturbation is expected because the perturbation field caused by the eddy currents increases with the size of the perturbation. The standard deviation of the SCR (Scharfetter *et al* 2003) at 100 kHz of our MIT-channel is shown for comparison and lies around 1.2×10^{-7}. This means that a central perturbation with a diameter of about 40 mm and a contrast of 2 with respect to the background can be resolved.

4. Discussion

Special software for segmentation, interactive modelling and simulation has been developed for real human geometries. It is possible to generate complex FE models and solve the eddy current problem. A 3D finite element model of the human brain with an oedema inside was generated and sensitivity maps were simulated for different sizes and positions of the oedema modelled as a spherical perturbation and of the coils.

The qualitative agreement between brain simulations and experimental and simulated results for a cylindrical model suggest that basic investigations concerning sensitivity distributions and electronic design can also be carried out with geometrically simple phantoms. Furthermore, simulations were carried out in order to find out which size of spherical perturbation within the brain is detectable with our MIT system. Thus, simulations with different sizes of perturbed sphere were performed and the calculated results were compared with our MIT-channel. The experimental error is difficult to quantify if movement artefacts are to be considered and the lower limit of the uncertainty of the SCR is still a matter of research. Some basic analysis has been done in Scharfetter *et al* (2003). We improved the equivalent

noise voltage density of our MIT-channel to 1 nV $Hz^{-1/2}$; thus a sphere with a diameter of circa 40 mm and contrast 2 in relation to the background can be resolved.

Taking into account that an oedema with a diameter of 40 mm is comparatively large, the choice of 100 kHz for the excitation frequency seems to represent the lower end for a spectroscopy system. At 100 kHz the sensitivity is considerably low while increasing linearly with the frequency. Hence, applying multi-frequency measurements (Scharfetter *et al* 2003), the detectability can be improved significantly.

Taking these results together, the detection of oedema in the human brain by MIT appears feasible. The present modelling and simulation environment will be used for tackling the complete inverse problem of MIT.

Acknowledgment

This work was supported by the Austrian Science Foundation FWF, project P14990.

References

Biro O 1999 Edge element formulations of eddy current problems *Comput. Methods Appl. Mech. Eng.* **160** 391–405

Gabriel S, Lau R W and Gabriel C 1996 The dielectric properties of biological tissues: III. Parametric models for the dielectric spectrum of tissues *Phys. Med. Biol.* **41** 2271–93

Griffiths H 2001 Magnetic induction tomography *Meas. Sci. Technol.* **12** 1126

Griffiths H, Steward W R and Gough W 1999 Magnetic induction tomography: a measuring system for biological tissues *Ann. NY Acad. Sci.* **873** 335–45

Hollaus K, Magele C, Brandstätter B, Merwa R and Scharfetter H 2002 Numerical simulation of the forward problem in magnetic induction tomography of biological tissue *Proc. 10th IGTE Symp. 2002*

Kao H P, Shwedyk E and Cardoso E R 1991 Measurement of canine cerebral oedema using vector impedance methods *Neurol. Res.* **13** 233–6

Korjenevsky A and Cherepenin V 1999 Progress in realization of magnetic induction tomography *Ann. NY Acad. Sci.* **873** 346–52

Korjenevsky A, Cherepenin V and Sapetsky S 2000 Magnetic induction tomography: experimental realization *Physiol. Meas.* **21** 89–94

Lingwood B, Dunster K, Colditz P and Ward L 2002 Noninvasive measurement of cerebral bioimpedance for detection of cerebral edema in the neonatal piglet *Brain Res.* **954** 97–105

Merwa R, Hollaus K, Brandstätter B and Scharfetter H 2003 Numerical solution of the general 3D eddy current problem for magnetic induction tomography (spectroscopy) *Physiol. Meas.* **24** 545–54

Netz J, Forner E and Haagemann S 1993 Contactless impedance measurement by magnetic induction—a possible method for investigation of brain impedance *Physiol. Meas.* **14** 463–71

Peyton A J, Yu Z Z, Al-Zeibak S, Saunders N H and Borges A R 1995 Electromagnetic imaging using mutual inductance tomography: potential for process applications *Part. Syst. Charact.* **12** 68–74

Scharfetter H, Casañas R and Rosell J 2003 Biological tissue characterization by magnetic induction spectroscopy (MIS): requirements and limitations *IEEE Trans. Biomed. Eng.* **50** 870–80

Scharfetter H, Riu P, Populo M and Rosell J 2002 Sensitivity maps for low-contrast perturbations within conducting background in magnetic induction tomography *Physiol. Meas.* **23** 195–202